Near Edge X-ray Absorption Fine Structure Spectroscopy of Bacterial Hydroxamate Siderophores in Aqueous Solutions

David C. Edwards*,† and Satish C. B. Myneni‡,§

Department of Chemistry, Princeton University, Frick Laboratory, Princeton, New Jersey 08544, Department of Geosciences, Guyot Hall, Princeton University, Princeton, New Jersey 08544, and Earth Sciences Division, Lawrence Berkeley National Laboratory, Berkeley, California 94720

Received: February 24, 2006; In Final Form: July 5, 2006

X-ray absorption spectroscopy (XAS) is widely used to explore the coordination environments and structures of metal complexes in aqueous solutions and disordered phases. Although soft-XAS studies on gaseous phases, solid phases and their interfaces have shown that XAS is a versatile tool in studying the functional group composition of organic molecules, the application of XAS to studying aqueous solutions is seriously limited because of experimental difficulties. In this report, using a modified synchrotron endstation geometry, we show how soft-XAS was used to study the changes in electronic states of reactive functional groups in a bacterial macromolecule, desferrioxamine B (desB, a hydroxamate siderophore) and its structural analogue (acetohydroxamic acid (aHa)). We collected C, N, and O near edge X-ray absorption fine structure (NEXAFS) spectra of these molecules in aqueous solutions and complemented their spectral interpretation with calculated X-ray spectra of "hydrated" aHa. The experimental spectra of desB are similar to those for aHa at the C, N, and O K-edges. In addition, the electronic transitions of amide and hydroxamate functional groups in the macromolecule can be distinguished from the N spectra. Small energy differences in the $\pi^*_{(C=O)NO}$ and the σ^*_{NO} transitions at the C- and N-edges of aHa and desB indicate that the substituent attached to N in desB ($(CH_2)_n$) determines the electron density in the (C═O)NO core. As the solution pH increased, the $\pi^*_{(C=O)NO}$ transition of the hydroxamate group of these two molecules exhibit energy shifts at the C-, N-, and O-edges, which are consistent with increased electron delocalization in the (C═O)NO core of aHa (and desB), predicted from the calculations. The spectra of the $aHa(H_2O)_3^-$ anion also provide evidence for partial N-deprotonation at pH values usually attributed to an O-acid. These results indicate that soft-XAS is well suited for studying the electronic states of different functional groups in aqueous organic macromolecules.

Introduction

Near edge X-ray absorption fine structure (NEXAFS) spectroscopy is rapidly becoming a commonly used technique to determine the functional group chemistry (composition, electronic states, proton and metal complexation) of complex organic macromolecules.[1−7] The element-specificity of this technique is useful in studying the functional group chemistry of macromolecules in heterogeneous matrixes.[6] However, direct probing of aqueous solutions and environmental samples is limited because of strong absorption of soft X-ray photons by air. The X-ray transmission, for example, is less than 5×10^{-4} for photons traveling one centimeter through air at atmospheric pressure at the C-edge. The construction of high flux and high brightness third generation synchrotron radiation sources in the past decade, combined with advances in X-ray endstation technology, have made in-situ soft X-ray NEXAFS spectroscopic studies of aqueous samples feasible.[8−11] Here, we show how NEXAFS spectroscopy was used to probe the functional group chemistry of aqueous biomacromolecules, such as siderophores.

Siderophores are organic macromolecules secreted by bacteria under iron limiting conditions to complex ferric iron.[12] Ubiquitous in the soil rhizosphere[13] and marine[14] systems (concentrations range from micromolar to nanomolar, respectively), siderophores effectively complex ferric iron because of their high binding constants (5−30 orders of magnitude higher than those for other common organic ligands).[15] The hydroxamate and phenolate functional groups in these molecules are responsible for this high reactivity and specificity for iron. Because of their affinity for iron, siderophores are also used in the treatment of siderosis.[16] Since researchers have shown that siderophores exhibit high affinity for other cations, siderophores are also considered as potential sequestration agents for actinides at radioactive waste repositores.[17,18] Although vibrational spectroscopic studies have been conducted on siderophores in aqueous solutions, the size and complexity of siderophores made them difficult to draw conclusions about the electronic state and structural environments of the reactive groups and their variation as a function of pH.[19]

Carbon and oxygen NEXAFS spectroscopic studies have been conducted on the functional group chemistry of many gas and solid-phase organic molecules, and trends have been established with regard to the influence of electron withdrawing/donating substituents on NEXAFS spectral shifts.[1,3,8,20,21] Although these studies are limited to molecules other than hydroxamates in the gaseous and solid states, information presented there is useful for addressing the electronic structure of the hydroxamate group in siderophores in aqueous solutions. Spectroscopic studies at

* Corresponding author. E-mail: dedwards@weslyancollege.edu.
† Department of Chemistry, Princeton University.
‡ Department of Geosciences, Princeton University.
§ Lawrence Berkeley National Laboratory.

10.1021/jp0611976 CCC: $33.50
Published on Web 09/29/2006

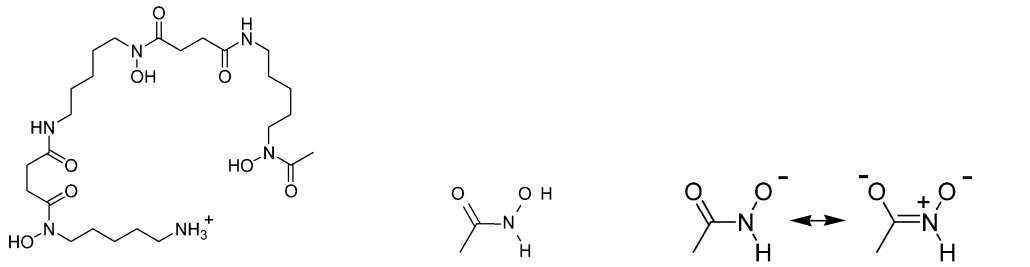

a. Desferrioxamine B b. *cis*-acetohydroxamic acid c. Resonance forms of aHa-*cis*-anion

Figure 1. Graphical representations of desB and aHa: (a) desferrioxamine B; (b) *cis*-acetohydroxamic acid; (c) resonance forms of *cis*-aHa deprotonated at the hydroxyl group.

the nitrogen K-edge, however, are less common. Recent studies have given conflicting results with the assignation of certain transitions, specifically for the σ^*_{N-H} and $\pi^*_{(C=O)NH}$ transitions, both of which are important in understanding the functional group chemistry of several biological macromolecules including proteins.[9,22,23] Through a comparison of experimental and calculated NEXAFS spectra, we report a set of guidelines for consistent interpretation of the spectral features at the nitrogen K-edge.

This study focuses on the chemical states of reactive functional groups in desferrioxamine B (desB), a common hydroxamate siderophore in the environment, and their variation as a function of pH in aqueous solutions (Figure 1). This molecule has four proton dissociation constants (pK_a) at 8.3, 9.0, 9.46, and 10.84, which correspond to successive deprotonation of the three hydroxamate groups (NOH) and the amine group (NH_3^+), respectively.[24] To complement the desB measurements, a smaller hydroxamate siderophore analogue, acetohydroxamic acid (aHa; Figure 1) with the same reactive functional group as desB, was also selected. Acetohydroxamic acid has a single proton dissociation constant (pK_a) at 9.37.[25] Information on the electronic structure variations of the hydroxamate functional group as a function of pH is necessary to understand the behavior of siderophores in aqueous solutions, and to design new molecules that exhibit high affinity for selected cations. The NEXAFS spectra of these small chains and macromolecules can provide this critical information. The experimental NEXAFS spectra of aHa are strengthened by theoretical calculations that aided in the interpretation of the electronic transitions and in the evaluation of the electronic structure of the different moieties. This study will expand the current small database of NEXAFS spectra of different functional groups in aqueous organic molecules and will assist in studying larger multifunctional organic macromolecules in biological systems.[6,26]

Experimental Details

Samples. Aqueous solutions of acetohydroxamic acid (Sigma Aldrich), desferrioxamine B (Sigma Aldrich), NaOH (Fisher Scientific), and HCl (Sigma Aldrich) were prepared gravimetrically with high purity 18 MΩ cm^{-1} water (Milli-Q Plus, Millipore). For the NEXAFS spectroscopic studies, solutions of 1.0 (±0.02) and 0.1 (±0.02) M aHa and 0.4 (±0.02) and 0.050 (±0.02) M desB were prepared and pH adjusted by the addition of 0.2 and 1.0 M NaOH or HCl. A high concentration of organic molecules was necessary for collecting the carbon and oxygen NEXAFS spectra to avoid interference from carbon contamination in beamline and from spectral contributions from water, respectively. However, this was not an issue at the N-absorption edge and dilute samples could be used for the N-NEXAFS spectral collection. The sample pH was measured using an Orion 525A pH meter fitted with a pH microprobe (accuracy of 0.01 pH). The samples were stored at 4 °C until used to avoid any pH variations that could occur at room temperature.

Instrumentation. All experiments were performed on beamline 8.0 at the Advanced Light Source, Lawrence Berkeley National Laboratory, using the soft X-ray endstation for environmental research (SXEER1; Figure 2a). This synchrotron beamline endstation was designed specifically for studying aqueous samples because the sample chamber could be maintained at atmospheric pressure (760 Torr). To achieve the atmospheric pressure in the sample chamber, a 0.16 μm thick silicon nitride (Si_3N_4) window was placed between the sample chamber and the ultrahigh vacuum part of the beamline. The sample chamber was filled with research-grade helium (purity ~99.99999%) to improve the transmission and to remove any spectral contamination from N_2, O_2, and CO_2. Inside the sample chamber, aqueous solutions were placed in a polypropylene straw (25 mm long, 8 mm diameter), with a 10 × 2 mm wedge cut into the straw to expose the sample directly to the photon beam (see Figure 2b). The sample was placed approximately 3 mm from the silicon nitride window. Each sample was scanned 10 times to ensure consistency and averaged together to improve the signal-to-noise ratio. The aqueous solutions in the sample holder were replenished after every five scans to mitigate the effect of beam damage and water evaporation (details provided below). The absorption spectra were recorded by detecting fluorescence photons with a gallium arsenide or a silicon photodiode. Spectral calibrations were also conducted for aHa at the beamline 11.0.2, using the scanning transmission X-ray microscope.

Carbon Edge. Spectra at the carbon edge were acquired from 270 to 320 eV with a 0.2 eV step size in the pre-edge (270−283 eV) and post-edge (295−320 eV) regions, and with a 0.05 eV step size in the edge region (283−295 eV). A 380 lines/mm grating monochromator was used with the entrance and exit slits set to 50 μm. With these slit openings, the resolution at the carbon edge is 0.2 eV (resolving power of 6600 with 10 μm slits). The raw fluorescence spectra were divided by incident photon intensity (I_o), measured simultaneously with sample fluorescence on gold mesh, to minimize spectral noise associated with fluctuations in the incident beam. The scattering contributions from water were removed from the aqueous sample spectra by subtracting the spectrum of pure water. The universal contamination of vacuum beamlines by adventitious carbon limited NEXAFS spectroscopy investigation of aqueous solutions at the C-edge to concentrated samples and the spectral interpretation to the pre-edge region only. The beam damage was negligible in these samples and this was evident from the spectral invariance in consecutive scans. All spectra were calibrated with reference to the 1s → π^* transition in carbon dioxide at 290.7 eV.[27]

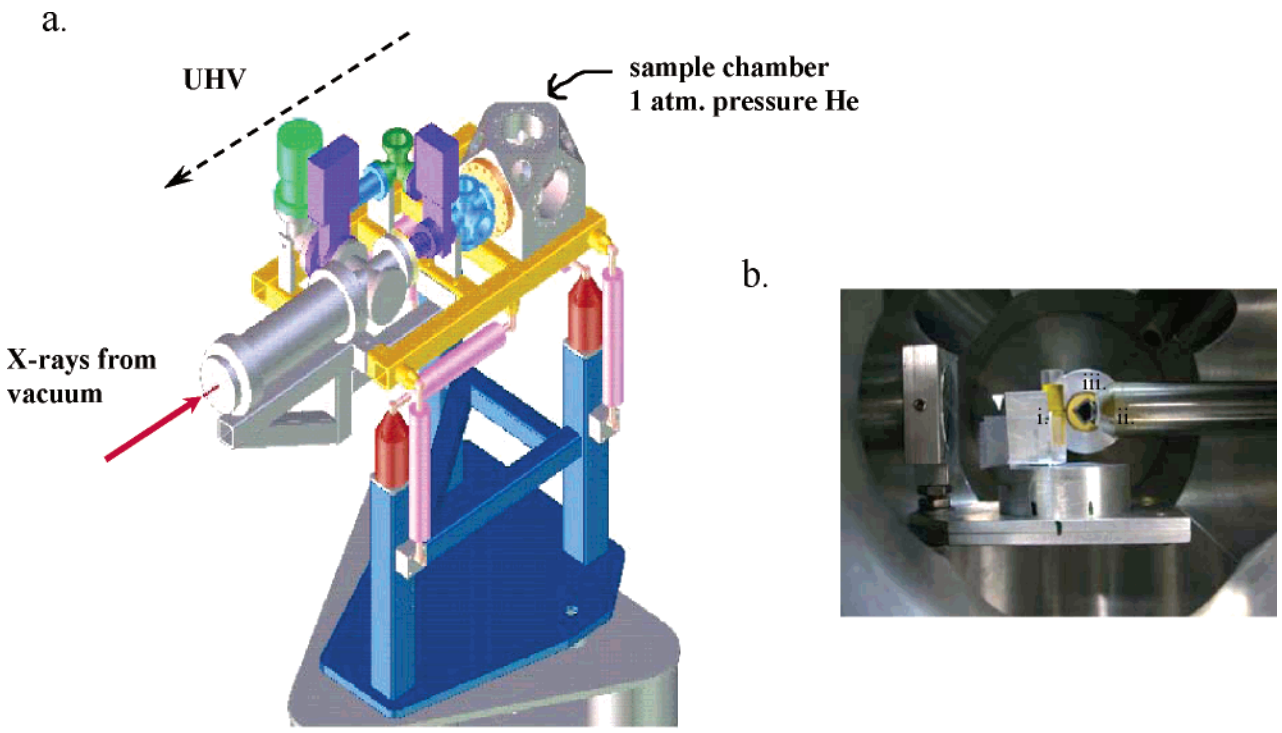

Figure 2. Schematic diagram of the soft X-ray endstation for environmental research (SXEER1) in (a), with the enlarged view of sample chamber in (b). (a) The sample chamber in SXEER1 is separated from the UHV section using a Si_3N_4 window. (b) The samples are placed in a polypropylene straw (i), which is about 3 mm away from the window (ii) during the measurement (the sample was moved back to show the detector (iii) behind).

Nitrogen Edge. Spectra at the nitrogen edge were collected from 390 to 430 eV for aHa and 395−425 eV for desB with a 0.2 eV step size in the pre-edge (390−395 eV) and post-edge (410−430/425 eV) regions, and with a 0.05 eV step size in the edge region (395−410). A 380 lines/mm grating monochromator was also used for collecting the N-NEXAFS spectra. The entrance and exit slits were set to 50 μm for aHa (resolution, 0.3 eV) and were closed to 25 μm for desB (resolution, 0.1 eV) to avoid beam damage. Sample decay was noticeable for desB after the first scan when the slits were set to 50 μm. The sample decay was indicated by increased intensity in the pre-edge transitions and by the appearance of new pre-edge features that occurred as a function of time. However, this was not the case when the slits were closed to 25 μm. In addition, the samples were replaced often with a fresh sample. The N-NEXAFS spectra were normalized as described above for the C-spectra, and the energy was calibrated using the second vibration of 1s $\rightarrow$ π^* transition of N_2 gas at 401.1 eV.[28]

Oxygen Edge. Spectra at the oxygen edge were acquired from 520 to 560 eV with 0.2 eV steps in the pre-edge (520−528 eV) and post-edge (540−560 eV) regions, and 0.05 eV steps in the edge region (528−540 eV). The entrance and exit slits were set at 50 μm for both aHa and desB solutions (resolution, 0.4 eV). The double normalization procedure, described above for C and N, was difficult for the O-edge spectra because of spectral contributions from O in water. Therefore, the 1s $\rightarrow$ π^* transitions in the pre-edge region were evaluated at the oxygen edge because these features did not have any interference from the water spectral features. Spectral variations between consecutive scans of a sample were small, which indicated that beam damage was negligible. The 1s $\rightarrow$ $2p\pi_g$ transition of O_2 at 530.8 eV was used for energy calibration.[29]

Peak Fitting. The overlapping peaks in the spectrum were fitted to get energies and peak heights of individual peaks using the software Peak Fit (Jandel Scientific, CA). The pre-edge and post-edge transitions were fit with Gaussian functions, whereas the edge was modeled with an arctangent function. The inflection of the arctangent was held constant at 290, 403, and 534 eV for the C-, N-, and O-edges, respectively. Because of the difficulties with normalization at the carbon and oxygen edges, only the pre-edge transitions were fit with confidence ($\pm$0.1 eV) by the iteration procedure in PeakFit.

DFT Calculations. The geometries of aHa$(H_2O)_3$ were optimized at the DFT B3LYP/ 6-31G* level of theory using Gaussian 92.[30] Three water molecules were used in the binding pocket to mimic an aqueous environment in the gas-phase calculations (Figure 3). Gas-phase aHa without water molecules did not simulate the experimental spectra well because electron localization effects were more amplified in a water-free structure, leading to transition energies that were inconsistent with our experimental results.[19] The *cis*-aHa$(H_2O)_3$ model was used to model the neutral structure because this structure was more stable than the *trans*-aHa$(H_2O)_3$ model. Similarly, O and N-deprotonated anionic structures of *cis*-aHa$(H_2O)_3^-$ were used because of their greater stability.[19] A gas-phase calculation for hydroxylamine (H_2NOH, without surrounding water molecules), was geometry optimized with StoBe[31] and used to aid in the interpretation of the σ^*_{N-O} transition at the nitrogen K-edge. The local basis set of the DFT code StoBe[31] was used to compute NEXAFS spectra for the geometry optimized models by using the gradient corrected exchange functional by Becke,[32] and correlation functional by Perdew.[33] The NEXAFS spectra were computed using the transition potential method[34] where both core and valence relaxation effects were approximated by putting half a core hole on the excited atom. The C, N, and O atoms were described by the IGLO-III[35] basis set, which gives a good description of the core orbitals. The core hole was localized at a given atom using effective core potentials (ECPs)[36] on the other atoms of the same type. A large diffuse basis set was added to the excited atom in a second step of the calculation

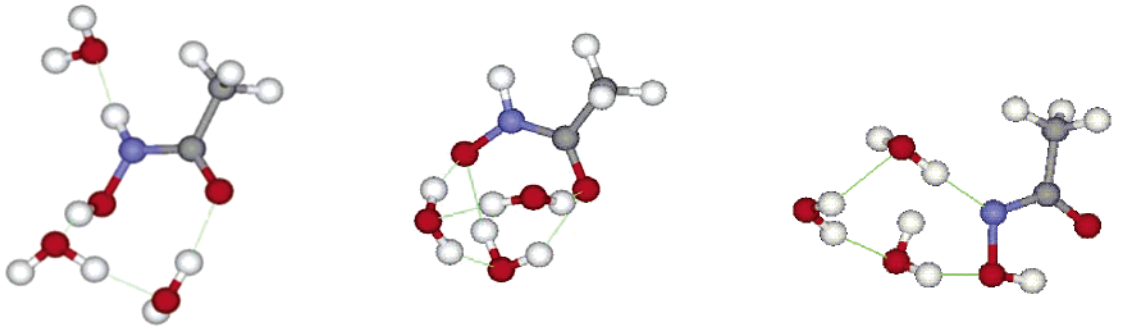

Figure 3. Calculated aHa models: (a) *cis*-aHa(H_2O)$_3$; (b) *cis*-aHa(H_2O)$_3$ O-anion; (c) *cis*-aHa(H_2O)$_3$ N-anion.

to better represent the Rydberg states and continuum part of the spectrum.[34]

The oscillator strengths were computed for the transitions between the core orbital and unoccupied states within the dipole approximation, using orbitals computed from the transition potential calculations for both the initial and final states. The orbital energy difference was used as the transition energy. The absolute energy scale was shifted to match the IP computed with higher accuracy using the ΔKohn−Sham approach.[37] In this approach, the IP is obtained by computing the difference in total energy between the ground state and a one-electron core hole excited state. The computed value of the IP was further improved by adding a relativistic correction,[37] which is 0.2 eV for carbon, 0.3 eV for nitrogen, and 0.4 eV for oxygen. The energy values after the correction fall within 0.2 eV of those in the experimental spectra. The calculated spectra were analyzed with the software package Molden, which was used in visualizing molecular orbital representations for each calculated transition.[38]

Results and Discussion

Protonation and deprotonation of aHa and desB associated with solution pH changes affect the electronic state of the reactive hydroxamate ((C═O)NO) moiety, and the spectral variations in the pre-edge regions of the C-, N-, and O-NEXAFS spectra depict this clearly. The experimental spectral variations are complemented by DFT calculated spectra for different species of aHa, and this information is used in the interpretation of different functional groups in desB.

Carbon K-Edge. The experimental C-NEXAFS spectra of aHa in aqueous solutions (Figure 4, Table 1) are compared to the calculated spectra of aHa models (Figure 4, Table 2). The 1s → $\pi^*_{(C=O)NO}$ transition for the protonated and deprotonated hydroxamate group of aHa is at 288.5 and 288.3 eV, respectively (Figure 4, Table 1). This red shift is indicative of a greater delocalization of electronic charge in the anion than in the neutral form of aHa, and this observation is also supported by a previous vibrational spectroscopic study.[19] A similar red shift was also observed in the case of deprotonation of carboxylic acid group in amino acids.[9] The calculated $\pi^*_{(C=O)NO}$ transitions are at 288.2, 288.2, and 288.1 eV for aHa(H_2O)$_3$, aHa(H_2O)$_3^-$ (O-anion), and aHa(H_2O)$_3^-$ (N-anion), respectively (Table 2). The electron delocalization caused by deprotonation is verified by the molecular representations that show an increased π character on the N−O bond in N- and O-deprotonated aHa models (Table 2). The calculated model for aHa(H_2O)$_3$ indicates that $\sigma^*_{CNO(oxime)}$ should occur at 290.8 eV. However, it is difficult to determine whether a shoulder at ∼289 eV in the experimental spectrum corresponds to this transition (Figure 4). Spectral normalization at the C-edge, as discussed earlier, limits the accurate interpretation of these weak transitions.

Desferrioxamine B has two different types of carbonyls associated with the amide and the hydroxamate groups. In the protonated state, desB exhibits a $\pi^*_{(C=O)NO}$ transition at 288.4 eV (Figure 5, Table 1). Upon deprotonation of the hydroxamate groups, the transition shifts to 288.3 eV (Figure 5, Table 1). The energy shift is similar to that for aHa, but lower in magnitude (0.2 eV for aHa). The spectral overlap of the $\pi^*_{(C=O)NO}$ and $\pi^*_{(C=O)NH}$ transitions from the hydroxamate and amide groups in desB, respectively, limits their unequivocal identification and spectral shifts accurately. The high pH desB spectrum also has a well-resolved feature at 289.6 eV due to a σ^*_{CNH} transition of the deprotonated terminal amine group (Figure 1). This transition energy is typical of amine groups in amino acids[1] and may not be distinct in neutral desB because of the transition intensity or spectral normalization problems.

The $\pi^*_{(C=O)NO}$ transitions of the hydroxamate group in aHa and desB are comparable to those of the other functional groups containing C═O moieties. The transition energies of different carbonyls at the carbon edge vary according to the electron withdrawing or donating tendencies of the substituents attached to the carbon atom.[3] Highly electronegative substituents adjacent to the carbonyl group shift the 1s → π^* transition to higher energies. For example, the 1s → π^* transitions of ketone (carbonyl surrounded by two carbons), carboxyl (carbonyl surrounded by a carbon and an oxygen), and carbonate (carbonyl surrounded by two oxygens) carbonyl are at 286.8, 288.6, and 290.5 eV, respectively.[3,6] When compared to the 1s → π^* transitions of these moieties, the 1s → π^* transition of a carbonyl in a hydroxamate group is expected between a ketone and a carboxyl group. Further, the oxygen atom connected to N in the hydroxamate group is more electron withdrawing than the hydrogen in amides (carbonyl 1s → π^* is at 288.2 eV), which places the hydroxamate transition between an amide and a carboxyl functional group.

Nitrogen K-Edge. Acetohydroxamic acid and desB consist of different types of N (C−N, N−O, N−H) and all of them exhibit electronic transitions at different energies, which can be identified unambiguously (Figure 1). In addition, the $\pi^*_{(C=O)NO}$ transition from the electron delocalization in the hydroxamate core is expected in the N-NEXAFS spectra of these molecules. Desferrioxamine B exhibits the above transitions in addition to transitions from the amide ($\pi^*_{(C=O)NH}$) and amine (σ^*_{NH}) groups. A discussion of the experimental and theoretical

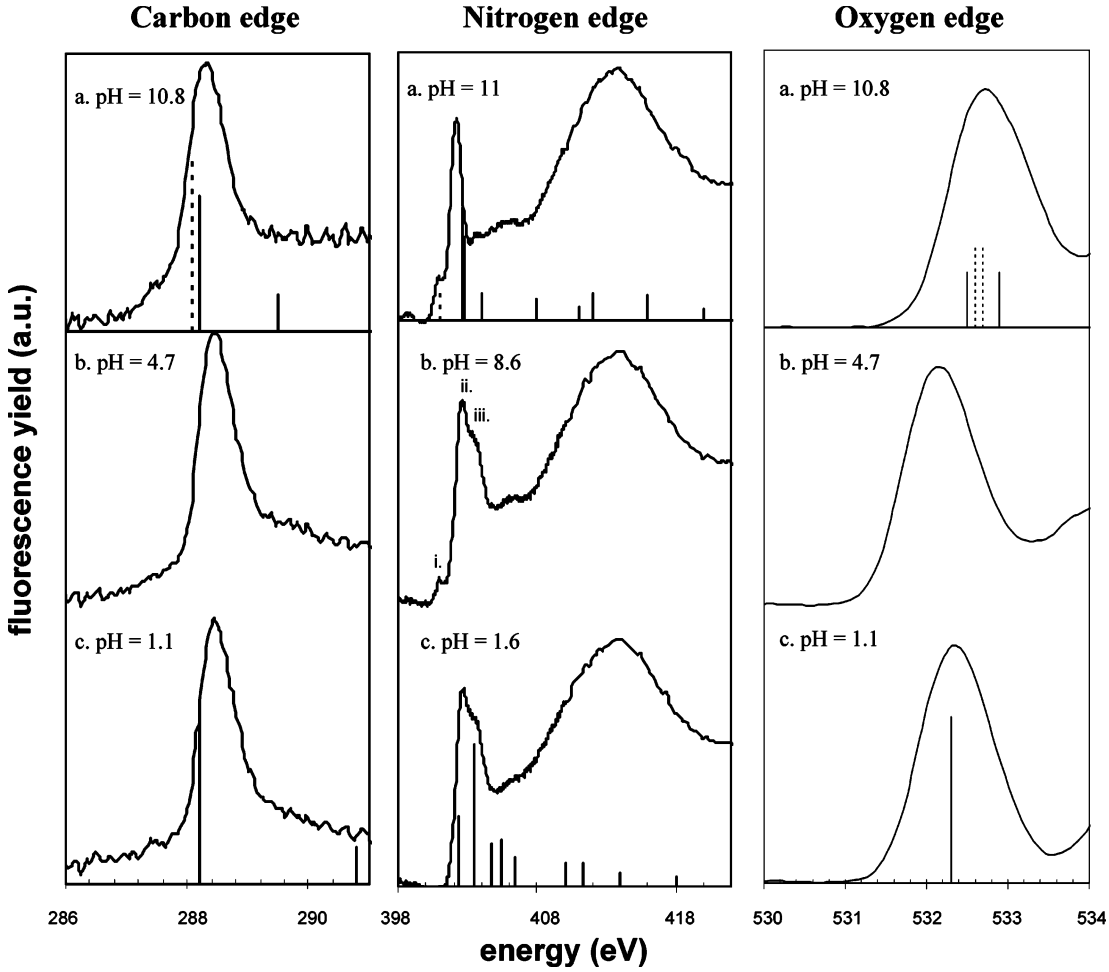

Figure 4. Experimental NEXAFS spectra of aHa at the C (1.0 M aHa), N (0.1 M aHa), and O (1.0 M aHa) absorption edges. Carbon edge: (a) pH = 10.8; (b) pH = 4.7; (c) pH = 1.1. Nitrogen edge: (a) pH = 11.0; (b) pH = 8.6 ((i) $\pi^*_{(C=O)NO}$; (ii) $\pi^*_{(C=O)NO}$; (iii) σ^*_{NO}); (c) pH = 1.6. Oxygen edge: (a) pH 10.8; (b) pH = 4.7; (c) pH = 1.1. Relative intensities of different 1s electronic transitions of the calculated models (neutral, O-anionic, and N-anionic aHa) are shown as vertical lines (solid vertical lines associated with all low pH spectra are calculated for neutral aHa; solid and dashed vertical lines for alkaline spectra represent the O-anion and N-anion, respectively).

work conducted at the N-edge is presented below, followed by spectral assignments in relation to the literature.

The experimental N-NEXAFS spectrum of neutral aHa exhibits intense peaks at 402.5 and 403.5 eV (Figure 4; Tables 1 and 3), consistent with calculated values (Figure 4). These are assigned to the $\pi^*_{(C=O)NO}$ and σ^*_{N-O} transitions, respectively. As the hydroxamate group in aHa deprotonates, the peak at 402.5 eV (Table 3) shifts to 402.2 eV whereas the intensity of the other (403.5 eV) drops significantly. A small "pre-edge" transition at 400.9 eV also appears for deprotonated aHa. The changes in these spectra are attributed to deprotonation at different sites in aHa: O-deprotonation and N-deprotonation. The changes of the peaks at 402.5 (energy shift) and 403.5 eV (intensity decrease) are attributed to deprotonation at the O-site, which changes the electron delocalization in the (C═O)NO core. Appearance of a new pre-edge peak at 400.9 eV, assigned to the $\pi^*_{(C=O)NO}$ transition, for aHa in alkaline solutions is attributed to the presence of N-deprotonated aHa, which is confirmed by the calculations. (Figure 4, Table 3). In addition to the above features, the N-NEXAFS spectra exhibit high-energy features at ∼406 and ∼414 eV, which are assigned to the σ^*_{N-H} and σ^*_{N-C} transitions, respectively. These peaks do not change as the solution pH is changed. Even if there are small variations in these broad spectral features, they are probably masked by water scattering contributions in the postedge region.

The calculated spectra of neutral aHa are consistent with the experimental observations, but the calculations of O-anion deviate from the experimental data. The discrepancy for the O-anion are related to the energy shifts of the $\pi^*_{(C=O)NO}$ and σ^*_{N-H} transitions (Figure 4, Table 3), which may have been caused by the significant localization of electron density on the N−H bond (specifically, on the hydrogen atom) in the O-anion model. Also, the calculated O-anion cannot account for the pre-edge transition in the experimental spectra at high pH (Figure 4). However, the calculations of the N-anion indicate that a combination of $\pi^*_{(C=O)NO}$ and σ^*_{N-O} exhibit transitions at 400.9 eV (Figure 4; Tables 1 and 3). This suggests that a small fraction of aHa may undergo deprotonation at the nitrogen atom. Because the oscillator strengths for the $\pi^*_{(C=O)NO}$ transition in the neutral, O-anion, and N-anion are similar (∼0.008, 0.01, 0.01, respectively), the O-anion may be considered as the dominant species in basic solutions because of the spectral intensity of the band at 402.2 eV being greater than the pre-edge feature at 400.9 eV.

The N-NEXAFS spectra of desB in acidic solutions exhibit two discrete peaks at 401.2 and 402.6 eV in the pre-edge region (Figure 5, Table 1). The low energy peak at 401.2 eV, attributed to the $\pi^*_{(C=O)NH}$ transition of the amide group, did not shift with changes in solution pH. The high energy peak at 402.6 eV, assigned to the $\pi^*_{(C=O)NO}$ of the hydroxamate group, shifts to

TABLE 1: Absolute Energies, Amplitudes, fwhm and Assignments for the Experimental Spectra of aHa and desB

pH	energy (eV)	aHa amp.[a]	fwhm (eV)[b]	assignment	pH	energy (eV)	amp.[a]	fwhm (eV)[b]	assignment
				Carbon					
1.1	288.1	0.5	3.7	σ^*_{C-H}	4.4	288.4	1	0.6	$\pi^*_{(C=O)NO}$
	288.5	3	0.6	$\pi^*_{(C=O)NO}$		289.5	0.4	1.9	σ^*_{CNH}
	289.1	0.9	1.6	$\sigma^*_{CNO(oxime)}$					
4.7	288.5	2.3	0.6	$\pi^*_{(C=O)NO}$	13.2	288.3	1	0.6	$\pi^*_{(C=O)NO}$
	289.1	0.9	2.2	$\sigma^*_{CNO(oxime)}$		289.6	0.9	2.9	σ^*_{CNH}
10.8	288.3	1.6	0.6	$\pi^*_{(C=O)NO}$					
	288.8	0.9	2.1	$\sigma^*_{CNO(oxime)}$					
				Nitrogen					
1.6	402.5	1	0.9	$\pi^*_{(C=O)NO}$	4.9	401.2	0.4	0.7	$\pi^*_{(C=O)NH}$
	403.5	0.7	1.3	σ^*_{NO}		402.6	0.6	0.8	$\pi^*_{(C=O)NO}$
						403.3	0.2	0.9	σ^*_{NO}
8.6	401.1	0.1	0.6	$\pi^*_{(C=O)NO}$	8.2	401.2	0.4	0.8	$\pi^*_{(C=O)NH}$
	402.5	1.2	1	$\pi^*_{(C=O)NO}$		402.5	0.5	0.8	$\pi^*_{(C=O)NO}$
	403.6	0.6	1.1	σ^*_{NO}		403.2	0.1	0.9	σ^*_{NO}
11.0	400.9	0.3	0.6	$\pi^*_{(C=O)NO}$	10.3	401.2	0.3	0.8	$\pi^*_{(C=O)NH}$
	402.2	1.5	1	$\pi^*_{(C=O)NO}$		402.3	0.6	0.9	$\pi^*_{(C=O)NO}$
				Oxygen					
1.1	532.4	1.7	1	$\pi^*_{(C=O)NO}$	4.4	532.3	1.2	0.9	$\pi^*_{(C=O)NO}$
4.7	532.2	2.1	1	$\pi^*_{(C=O)NO}$	13.2	532.5	1.1	1.1	$\pi^*_{(C=O)NO}$
	533.6	0.4	1.3	σ^*_{ON}					
10.8	532.7	1.5	1	$\pi^*_{(C=O)NO}$					
	533.4	0.2	0.6	σ^*_{ON}					

[a] Amplitudes for the experimental spectra were found using the fitting program PeakFit. [b] fwhm = full width at half-maximum.

TABLE 2: Calculated Energies and Proposed Assignments for aHa at the C K-Edge

Calculated energy (eV)	osl[b]	Assignment[a]	Calculated energy (eV)	osl[b]	Assignment[a]
$aHa(H_2O)_3$			$aHa(H_2O)_3^-$ O-anion		
288.2	0.032	$\pi^*_{(C=O)NO}$ 	288.2	0.027	$\pi^*_{(C=O)NO}$ 
			287.2		IP for methyl carbon
290.8	0.00094	$\sigma^*_{CNO(oxime)}$ 	288.6		IP for carbonyl carbon
			$aHa(H_2O)_3^-$ N-anion		
			288.1	0.028	$\pi^*_{(C=O)NO}$ 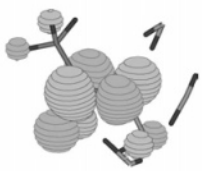
290.7		IP for methyl carbon			
293.2		IP for carbonyl carbon	286.7		IP for methyl carbon
			288.1		IP for carbonyl carbon

[a] Assignments are generated from the molecular orbital representations of the calculations transitions. [b] osl is used to indicate the sum of the oscillator strengths in the *x*, *y*, *z* directions for each transition energy.

402.3 eV upon deprotonation. This 0.3 eV red shift is similar to the shift observed for aHa, with energies 0.1 eV higher due to increased electron delocalization in desB. In addition to these features, desB exhibited peaks at 403.3, 407, 410, and 414 eV in acidic solutions, which are assigned to the σ^*_{N-O}, σ^*_{N-H} (amine group), σ^*_{N-C} (amide group), and σ^*_{N-C} (hydroxamate group) transitions, respectively. As shown for aHa above, the peak at 403.3 eV disappears and the others remain unchanged as the sample pH is increased. The shift of the band at 402.6 eV in the case of aqueous desB is indicative of exclusively O-acid deprotonation because of similar spectral changes in aHa (Figure 4).

Because there are limited NEXAFS spectroscopic studies at the N-edge, details of peak assignments are provided below.

(a) $\pi^*_{(C=O)NH}$ *Transition.* Experimental and theoretical studies of formamide indicate that its $\pi^*_{(C=O)NH}$ transition is at

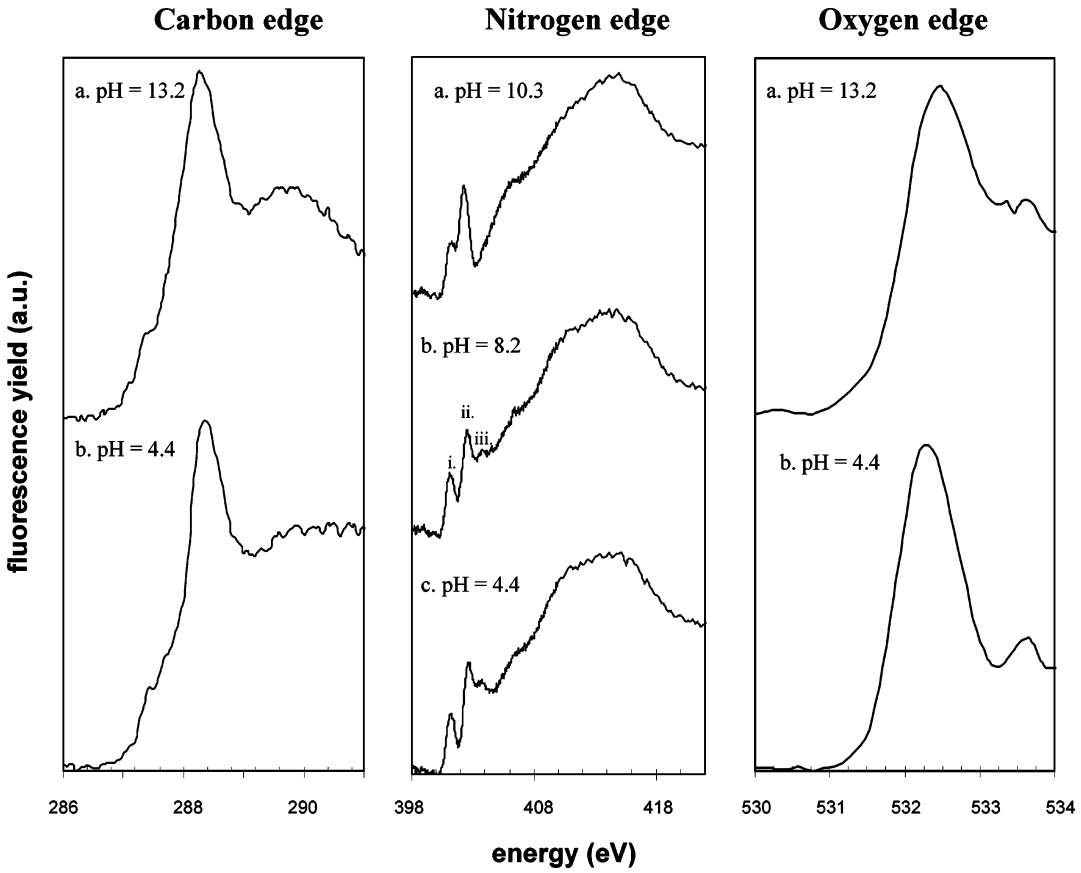

Figure 5. Experimental NEXAFS spectra of desB at the carbon (400 mM desB), nitrogen (50 mM desB), and oxygen (400 mM desB) absorption edges. Carbon edge: (a) pH = 13.16; (b) pH = 4.42. Nitrogen edge: (a) pH = 10.31; (b) pH = 8.24 ((i) $\pi^*_{(C=O)NH}$; (ii) $\pi^*_{(C=O)NO}$; (iii) σ^*_{NO}); (c) pH = 4.42. Oxygen edge: (a) pH = 13.16; (b) pH = 4.42.

401.9 eV.[22,39] However, the energy of this transition is influenced significantly by the substituents around the nitrogen atom and the bond strength of the carbonyl bond.[5,39] The attachment of an electron donating group to the amide nitrogen shifts the $\pi^*_{(C=O)NH}$ transition to a lower energy (e.g., a methylene group (CH_2) attachment in glycyl glycine shifts this transition to 401.5 eV),[22] whereas an electron withdrawing group shifts this transition to a higher energy (e.g., a glucose ring in *N*-acetyl-D-glucosamine shifts this transition to 402.5 eV).[5] On the basis of these spectral variations of models, the peak at 401.2 eV in desB is assigned to the electronic transitions of $\pi^*_{(C=O)NH}$ of amide group and the peak at ~402.6 eV is assigned to the electronic transitions of $\pi^*_{(C=O)NO}$ transition of hydroxamate groups in desB.

(b) σ^*_{N-O} *Transition.* To the best of our knowledge, compounds containing an oxime group (σ^*_{N-O}) have not been examined by NEXAFS spectroscopy. Our N-NEXAFS spectroscopic studies on a related smaller molecule, hydroxylamine (H_2NOH), indicate that its σ^*_{N-O} transition is at 402.0 eV (Figure 6).[40] Gas-phase calculations of hydroxylamine indicate that the σ^*_{N-O} transition is located at 402.5 eV and closely resembles the experimental spectrum of the solid powder. When compared to the case for hydroxylamine, the electron withdrawing carbonyl attached to the nitrogen in the hydroxamate group (compared to H in hydroxylamine) increases the energy of σ^*_{N-O} above 402.0 eV. Such high energy N−O transitions are also noticed in nitro and nitrate compounds (~405 eV), which have electron withdrawing groups adjacent to the nitrogen atom.[5] On the basis of these observations, we assigned the peaks around 403.5 eV for aHa and desB to σ^*_{N-O} transition.

(c) σ^*_{N-C} *Transition.* Amides and amines have different bonding environments when compared to those for the hydroxamate group, and this is also reflected in their σ^*_{N-C} transitions. This electronic transition occurs as a broad feature in the energy range 405−408 eV for amines, and around 410 eV for amides.[39,41,42] The NEXAFS spectral studies on amine groups in glycine[22] and alanine[43,44] and an ISEELS study on formamide[39] support the above assignments. The increase in energy in formamide when compared to that for the amine groups is due to the possible resonance structures in the amide group that cannot occur in the amine group. The characteristics of the hydroxamate group are more like those of an amide than those of an amine group. The transition at 414 eV in both aHa and desB is likely due to the σ^*_{N-C} hydroxamate transition, and the transition at 410 eV in desB is due to the σ^*_{N-C} amide transition.

(d) σ^*_{N-H} *Transition.* Gas-phase molecules containing amine groups (e.g., methylamines, glycine) exhibit low energy Rydberg state transitions below 405 eV, and σ^*_{N-H} transitions around 407 eV.[6,22,45−47] However, the Rydberg transitions disappear for molecules in condensed phases (e.g., glycine).[6,9,22,45,46] The σ^*_{N-H} transition is at 403.2 eV but is part of an oxime group, not an amine group (Figure 6). Hence, the broad feature around 407 eV in desB is assigned to the σ^*_{N-H} amine transition (Figure 5). Because the σ^*_{N-H} transitions of amide occur at energies similar to those for the σ^*_{N-H} transition in amines,[39] the amide σ^*_{N-H} transition is also expected around 407 eV.

Oxygen K-Edge. NEXAFS spectroscopic measurements of O-containing molecules are difficult in aqueous solutions because of strong spectral contributions from water. Hence, the O-NEXAFS spectroscopic studies of aHa and desB are limited

TABLE 3: Calculated Energies and Proposed Assignments for aHa at the N-Edge

Calculated energy (eV)	osl[b]	Assignment[a]
$aHa(H_2O)_3$		
402.3	0.0077	$\pi^*_{(C=O)NO}$
403.5	0.014	$\sigma^*_{NC}/\sigma^*_{N-O}$
404.7	0.0024	σ^*_{N-O}
405.4	0.00026	σ^*_{N-H}
406.4		IP for nitrogen atom
$aHa(H_2O)_3^-$ O-anion		
402.6	0.011	$\pi^*_{(C=O)NO}$
402.8	0.0031	σ^*_{N-H}
402.6		IP for nitrogen atom
$aHa(H_2O)_3^-$ N-anion		
401.1	0.0099	$\pi^*_{(C=O)NO}$
401.1	0.0037	σ^*_{N-O}
401.2	0.0093	σ^*_{N-O}
400.5		IP for nitrogen atom

[a] Assignments are generated from the molecular orbital representations of the calculations transitions. [b] osl is used to indicate the sum of the oscillator strengths in the *x*, *y*, *z* directions for each transition energy.

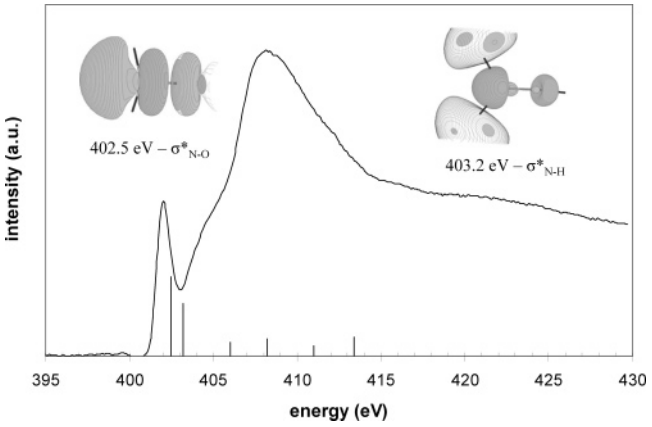

Figure 6. Experimental NEXAFS spectrum of hydroxylamine (solid) at the nitrogen absorption edge. Vertical lines represent calculated transitions for the σ^*_{N-O} and σ^*_{N-H} bands.

to the $\pi^*_{(C=O)NO}$ (and $\pi^*_{(C=O)NH}$ in the case of desB) transition, which occur below the water absorption edge.[8] The experimental O-NEXAFS spectra for aHa show that its $\pi^*_{(C=O)NO}$ transition is at 532.4 eV in acidic solutions, 532.2 eV at neutral pH, and 532.7 eV in alkaline solutions (Figure 4, Table 1). The calculated spectra support the experimental blue shift of the $\pi^*_{(C=O)NO}$ transition with deprotonation of the hydroxamate group (Figure 4, Table 4). This blue shift upon aHa deprotonation is opposite to the observation made at the carbon and nitrogen edges. This may be caused by increased electropositive character on the carbonyl oxygen atom. Upon deprotonation at the carbonyl oxygen, aHa loses electron density in the formation of the partial C═N bond (supported by our previous infrared spectroscopy study).[19] However, this is difficult to predict from the theoretical calculations because the relative shifts in the ionization potentials at the oxygen edge between neutral and anionic models are within the error of the calculation. Spectral shifts shown here for hydroxamate are similar to a blue shift observed for the deprotonation of the carboxylic acid group in glycine.[9] The amide and hydroxamate carbonyls in desB are difficult to distinguish because of stronger overlap of their electronic transitions.[3] The desB spectra exhibit a $\pi^*_{(C=O)NO}$ transition at 532.3 eV in acidic solutions, which shift to 532.5 eV upon deprotonation of desB (Figure 5, Table 1). This trend is similar to that for aHa.

Summary

The results presented here indicate that soft X-ray absorption spectroscopy is a versatile technique to identify different functional groups in organic molecules, their electronic states, and their variation as a function of solution pH. However, there are limitations with respect to the detection limits. The sensitivity for detecting C- and O-groups with the currently available detectors is low because of C contamination associated with synchrotron vacuum components and overlap with O-NEXAFS features of water, respectively. The presence of adventitious carbon on X-ray mirrors and focusing optics absorbs X-rays around 284 and 290 eV and produces features that are difficult

TABLE 4: Calculated Energies and Proposed Assignments for aHa at the O K-Edge

Calculated energy (eV)	osl[b]	Assignment[a]	Calculated energy (eV)	osl[b]	Assignment[a]
$aHa(H_2O)_3$			$aHa(H_2O)_3^-$ N-anion		
532.3	0.0099	$\pi^*_{(C=O)NO}$	532.6	0.0025	$\pi^*_{(C=O)NO}$
534.1	0.0003	σ^*_{ON}	532.7	0.0021	$\pi^*_{(C=O)NO}$
535.7	0.0039	$\pi^*_{OCN}/\sigma^*_{ON}$	534.7	0.0032	σ^*_{ON}
536.6		IP for carbonyl oxygen	534.9	0.0039	σ^*_{ON}
538.7		IP for oxime oxygen			
$aHa(H_2O)_3^-$ O-anion					
532.5	0.00018	$\pi^*_{(C=O)NO}$	536.2	0.0051	σ^*_{ON}
532.9	0.00013	$\pi^*_{(C=O)NO}$	532.1		IP for carbonyl oxygen
532.4		IP for carbonyl oxygen	534.2		IP for oxime oxygen
532.3		IP for oxime oxygen			

[a] Assignments are made by evaluating the molecular orbital representations of the calculated transitions. [b] osl is used to indicate the sum of the oscillator strengths in the *x, y, z* directions for each transition energy.

to normalize around these energies. Attempts are underway at several facilities to minimize this contamination. In addition, higher order harmonics at the C-edge increases spectral background, which primarily comes from the fluorescence of oxygen in water for aqueous solution samples. This increase in spectral background lowers the detection limits at the C-absorption edge. In the case of O-NEXAFS spectra, water exhibits strong absorption bands above ~534 eV and restricts organic molecule studies to the π^* transitions below these energies. However, the N-functional groups can be identified with sensitivities higher than those of the other two groups discussed above.

From this soft XAS study of aHa and desB, the following information could be summarized on their chemical state: (1) contrary to previous IR studies,[19] aHa appears to behave as a mixed acid, displaying characteristics of both an O-acid (majority of species at high pH) and a N-acid (minor species), (2) the electron density in the reactive (C═O)NO core for aHa and desB is highly delocalized, and (3) theoretical calculations on "hydrated" aHa aided in the interpretation of its experimental spectra, and in the evaluation of the electronic states of different functional groups in desB. This work on siderophores is directly applicable to studies that involve aqueous metal or surface complexation of organic molecules, as shown in a recent study.[26] Information on the intensity of electron delocalization in the (C═O)NO core of the reactive groups of aHa and desB can be used in identifying the mechanisms of aqueous and solid-phase iron complexation in the presence of bacterial siderophores.

These soft X-ray spectroscopy studies on aqueous organic molecules also clearly indicate that structural and electronic information of functional groups in macromolecules can be probed using information from smaller, structurally similar molecules. Recent studies involving the structure of humic substances,[6] peptide sequences,[1] microgels,[10] and metal−organic complexes[26] have shown that soft XAS is a promising method for environmental research.[6] However, without a concrete background on the spectral transitions of smaller organic compounds in aqueous solutions, this technique will not be amenable or practical for these studies. Also, theoretical calculations are integral for understanding the correct transitions that occur within these molecules.

Acknowledgments. This research was funded by the EMSP program of the Department of Energy, and NSF (Chemical Sciences). David C. Edwards also received funding from the Advanced Light Source doctoral fellowship and the Princeton Environmental Institute−Science, Technology, and Environmental Policy (PEI−STEP) fellowship. We thank Henrik Ostrom for assistance with the methods and interpretation of calculated spectra. We also thank J. Majzlan and A. Leri for comments on the manuscript.

References and Notes

(1) Kaznacheyev, K.; Osanna, A.; Jacobsen, C.; Plashkevych, O.; Vahtras, O.; Agren, H.; Carravetta, V.; Hitchcock, A. P. *J. Phys. Chem. A* **2002**, *106*, 3153.

(2) Chan, C. S.; DeStasio, G.; Weich, S. A.; Girasole, M.; Frazer, B. H.; Nesterova, M. V.; Fakra, S.; Banfield, J. S. *Science* **2004**, *303*, 1658.

(3) Urquhart, S. G.; Ade, H. *J. Phys. Chem. B* **2002**, *106*, 8531.

(4) Lawrence, J. R.; Swerhone, G. D. W.; Leppard, G. G.; Araki, T.; Zhang, X.; West, M. M.; Hitchcock, A. P. *Appl. Environ. Microbiol*. **2003**, *69*(9), 5543.

(5) Vairamurthy, A.; Wang, S. *Environ. Sci. Technol*. **2002**, *36*, 3050.

(6) Myneni, S. C. B. In *Rev. Mineral. Geochem.*, Fenter, P. A.; Rivers, M. L.; Sturchio, N. C.; Sutton, S. R., Eds. **2002**, 486.

(7) Stohr, J. *NEXAFS Spectroscopy*; Springer-Verlag: Heidelberg, 1992.

(8) Myneni, S.; Luo, Y.; Naslund, L. A.; Cavalleri, M.; Ojamae, L.; Ogasawara, H.; Pelmenschikov, A.; Wernet, Ph.; Vaterlein, P.; Heske, C.; Hussain, Z.; Pettersson, L. G. M.; Nilsson, A. *J. Phys.: Condens. Matter* **2002**, *14*, L213.

(9) Messer, B. M.; Cappa, C. D.; Smith, J. D.; Wilson, K. R.; Gilles, M. K.; Cohen, R. C.; Saykally, R. J. *J. Phys. Chem. B* **2005**, *109*, 5375.

(10) Fujii, S. F.; Armes, S. P.; Araki, T.; Ade, H. *J. Am. Chem. Soc*. **2005**, 127, 16808.

(11) Guay, D.; Stewart-Ornstein, J.; Zhang, X.; Hitchcock, A. P. *Anal. Chem.* **2005**, *77*, 3479.

(12) Neilands, J. B. *Annu. Rev. Biochem*. **1981**, *50*, 715.

(13) Powell, P. E.; Cline, G. R.; Reid, C. P. P.; Szanislo, P. J. *Nature* **1980**, *287*, 833.

(14) Martinez, J. S.; Zhang, G. P.; Holt, P. D.; Jung, H.-T.; Carrano, C. J.; Haygood, M. G.; Butler, A. *Science* **2000**, *287*, 1245.

(15) Raymond, K. N.; Carrano, C. J. *Acc. Chem. Res.* **1979**, *12*, 183.

(16) Harris, W. R.; Raymond, K. N. *J. Am. Chem. Soc.* **1979**, *101*, 6534.

(17) Brainard, J. R.; Strietelmeier, B. A.; Smith, P. H.; Langston-Unkefer, P. J.; Barr, M. E.; Ryan, R. R. *Radiochim. Acta* **1992**, *58*/*59*, 357.

(18) Kappel, M. J.; Nitsche, H.; Raymond, K. N. *Inorg. Chem*. **1985**, *24*, 605.

(19) Edwards, D. C.; Nielsen, S. B.; Jarzecki, A. A.; Spiro, T. G.; Myneni, S. C. B. *Geochim. Cosmochim. Acta* **2005**, *69*, 3237.

(20) Francis, J. T.; Hitchcock, A. P. *J. Phys. Chem*. **1992**, 6598.

(21) Urquhart, S. G.; Hitchcock, A. P.; Priester, R. D.; Rightor, E. G. *J. Polym. Sci.: Part B: Polym. Phys.* **1995**, *33*, 1603.

(22) Gordon, M. L.; Cooper, G.; Morin, C.; Araki, T.; Turci, C. C.; Kaznatcheev, K.; Hitchcock, A. P. *J. Phys. Chem. A* **2003**, *107*, 6144.

(23) Zubavichus, Y.; Zharnikov, M.; Schaporenko, A., Grunze, M. *J. Electron Spectrosc.* **2004**, *134*, 25.

(24) Farkas, E.; Enyedy, E. A.; Csoka, H. *Polyhedron* **1999**, *18*, 2391.

(25) Schwarzenbach G.; Schwarzenbach K. *Helv. Chim. Acta* **1963**, *46*, 1390.

(26) Edwards, D. C.; Myneni, S. C. B. *J. Phys. Chem A* **2005**, *109*, 10249.

(27) Sham, T. K.; Yang, B. X.; Kirz, J.; Tse, J. S. *Phys. Rev. A* **1989**, *40*, 652.

(28) Chen, C. T.; Ma, Y.; Sette, F. *Phys. Rev. A* **1989**, *40*, 6737.

(29) Hitchcock, A. P.; Brion, C. E. *J. Electron Spectrosc*. **1980**, *18*, 1.

(30) Frisch, M. J.; Trucks, G. W.; Head-Gordon, M.; Gill, P. M. W.; Wong, M. W.; Foresman, J. B.; Johnson, B. C.; Schlegel, H. B.; Robb, M. A.; Replogle, E. S.; Gomperts, R.; Andres, J. L.; Raghavachari, K.; Binkley, J. S.; Gonzalez, C.; Martin, R. L.; Fox, D. J.; Defrees, D. J.; Baker, J.; Stewart, J. J. P.; Pople, J. A. *Gaussian 92*, revision C; Gaussian Inc.: Pittsburgh, PA, 1992.

(31) Hermann, K.; Pettersson, L. G. M.; Casida, M. E.; Daul, C.; Goursot, A.; Koester, A.; Proynov, E.; St-Amant, A.; Salahub, D. R. Contributing authors: Carravetta, V.; Duarte, H.; Godbout, N.; Guan, J.; Jamorski, C.; Lebeouf, M.; Malkin, V.; Malkina, O.; Nyberg, M.; Pedocchi, L.; Sim, F.; Triguero, L.; Vela, A. *StoBe-deMon version 1.0*, deMon Software, 2002.

(32) Becke, A. D. *Phys. Rev. A* **1988**, *38*, 3098.

(33) Perdew, J. P. *Phys. Rev. B* **1986**, *34*, 7406.

(34) Triguero, L.; Pettersson, L. G. M. *Phys. Rev. B* **1998**, *58*, 8097.

(35) Pettersson, L. G. M.; Wahlgren, U.; Gropen, O *J. Chem. Phys.* **1987**, *86*, 2176.

(36) Kutzelnigg, W.; Fleischer, U.; Schindler, M. *NMR: Basic Principles and Progress*; Springer-Verlag: Heidelberg, Germany, 1990.

(37) Triguero, L.; Plashkevych, O.; Pettersson, L. G. M.; Agren, H. *J. Electron Spectrosc.* **1999**, *104*, 195.

(38) G.Schaftenaar; Noordik, J. H. *J. Comput.-Aided Mol. Design* **2000**, *14*, 123.

(39) Ishii, I.; Hitchcock, A. P. *J. Chem. Phys.* **1987**, *87*, 830.

(40) Solid hydroxylamine was purchased from Sigma-Aldrich. The solid powder spectrum at the N K-edge was obtained from beamline 6.3.1 at the ALS. Calibration was done by taking the shift at the carbon and oxygen edge at the same grating and dividing by 2. The energy resolution is ±0.2 eV.

(41) Sodhi, R. N. S.; Brion, C. E. *J. Electron Spectrosc*. **1985**, *36*, 187.

(42) Wight, G. R.; Brion, C. E. *J. Electron Spectros.* **1974**, *4*, 25.

(43) This group, unpublished results.

(44) Harshbarger, W. R.; Skerbele, A.; Lassettre, E. N. *J. Chem. Phys*. **1971**, *54*, 3784.

(45) Weiss, K.; Bagus, P. S.; Woll, Ch. *J. Chem. Phys*. **1999**, *111*, 6834.

(46) Steinberger, I. T.; Teodorescu, C. M.; Gravel, D.; Flesch, R.; Wassermann, B.; Reichardt, G.; Hutchings, C. W.; Hitchcock, A. P.; Ruhl, E. *Phys. Rev. B* **1999**, *60*, 3995.

(47) Urquhart, S. G.; Hitchcock, A. P.; Smith, A. P.; Ade, H.; Rightor, E. G. *J. Phys. Chem. B* **1997**, *101*, 2267.